Tetrahedron 65 (2009) 8021–8027

Contents lists available at ScienceDirect

Tetrahedron

journal homepage: www.elsevier.com/locate/tet

Visualization and quantification of anisotropic effects on the ^{1}H NMR spectra of 1,3-oxazino[4,3-*a*]isoquinolines—indirect estimates of steric compression

Erich Kleinpeter [a,*], István Szatmári [b], László Lázár [b], Andreas Koch [a], Matthias Heydenreich [a], Ferenc Fülöp [b]

[a] *Department of Chemistry, University of Potsdam, Karl-Liebknecht-Str. 24-25, D-14476 Potsdam(Golm), Germany*
[b] *Research Group for Stereochemistry, Hungarian Academy of Sciences—Institute of Pharmaceutical Chemistry, University of Szeged, Eötvös u. 6., H-6720 Szeged, Hungary*

ARTICLE INFO

Article history:
Received 10 June 2009
Received in revised form 9 July 2009
Accepted 17 July 2009
Available online 22 July 2009

Keywords:
Anisotropic effect
1,3-Oxazino[4,3-*a*]isoquinoline derivatives
NMR spectroscopy
Theoretical calculations
GIAO
Steric compression
^{1}H chemical shifts

ABSTRACT

The anisotropic effects of the phenyl, α- and β-naphthyl moieties in four series of 1,3-oxazino[4,3-*a*]-isoquinolines on the ^{1}H chemical shifts of the isoquinoline protons were calculated by employing the Nucleus Independent Chemical Shift (NICS) concept and visualized as anisotropic cones by a through-space NMR shielding grid. The signs and extents of these spatial effects on the ^{1}H chemical shifts of the isoquinoline protons were compared with the experimental ^{1}H NMR spectra. The differences between the experimental δ (^{1}H)/ppm values and the calculated anisotropic effects of the aromatic moieties are discussed in terms of the steric compression that occurs in the compounds studied.

1. Introduction

The shielding constant at or above the center of aromatic ring systems (a nucleus independent chemical shift—NICS)[1] can be used to characterize the aromaticity of organic compounds. NICS values on a grid around molecules can be calculated to locate the diatropic and paratropic regions of the molecules involved.[2] These through-space NMR shieldings (TSNMRSs) have been visualized[3] as isochemical-shielding surfaces (ICSSs) and employed to quantify the anisotropic effects of functional groups (to determine the stereochemistry of nuclei proximal to the functional group),[3–18] to separate the anisotropic effect of the C=C double bond from the influence of steric hindrance on the same protons,[19] and to visualize and quantify planar[20,21] and spherical (*anti*)aromaticity.[22–24]

Similar approaches to estimate TSNMRS have been published by Alkorta and Elguero,[25] and Martin et al.[26] In both cases, shieldings of similar size and direction, comparable with the results of our model and the classical model of Bovey and Johnson[27] and Haigh and Mallion,[28,29] were obtained.

Of significant note though, there have been some recent developments of the NICS index[30] showing that not the average NICS but only the NICS(1)$_{zz}$ component could rigorously be used to quantify aromaticity[31] and average NICS have proven to be not generally suitable for the quantitative evaluation of aromaticity.[32–34] For example, NICS analysis was shown to lead to an incorrect prediction of aromaticity,[33] e.g., for cyclopropane[34] and the cyclopropenyl anion.[35]

During the conformational analysis of several series of 1,3-oxazino[4,3-*a*]isoquinolines **1**–**4** (cf. Scheme 1),[36,37] the proton chemical shifts of the isoquinoline moiety proved to be strongly dependent on the oxazine part of the molecules. Besides the conformations of these compounds, therefore, both the anisotropic effect of the phenyl group (in **2**), and the α- (in **3**) and β-naphthyl group (in **4**) and the steric compression (the stronger the steric hindrance, the more the protons involved are shifted to low field) came into question. As we have considerable experience in employing TSNMRS grids for the visualization and quantification of anisotropic effects,[3–18] and hence separating these effects from competitive steric compression effects on the same proton chemical shifts,[10,19] our earlier approach[3] was applied and the anisotropic effects of the above aromatic moieties on the isoquinoline protons were quantified. A critical comparison of the experimental ^{1}H chemical shift variations in **1**–**4** with the anisotropic effects of the aromatic moieties in **2**–**4** should answer the given question.

* Corresponding author. Tel.: +49 331 977 5210; fax: +49 331 977 5064.
E-mail address: kp@chem.uni-potsdam.de (E. Kleinpeter).

0040-4020/$ – see front matter © 2009 Elsevier Ltd. All rights reserved.
doi:10.1016/j.tet.2009.07.038

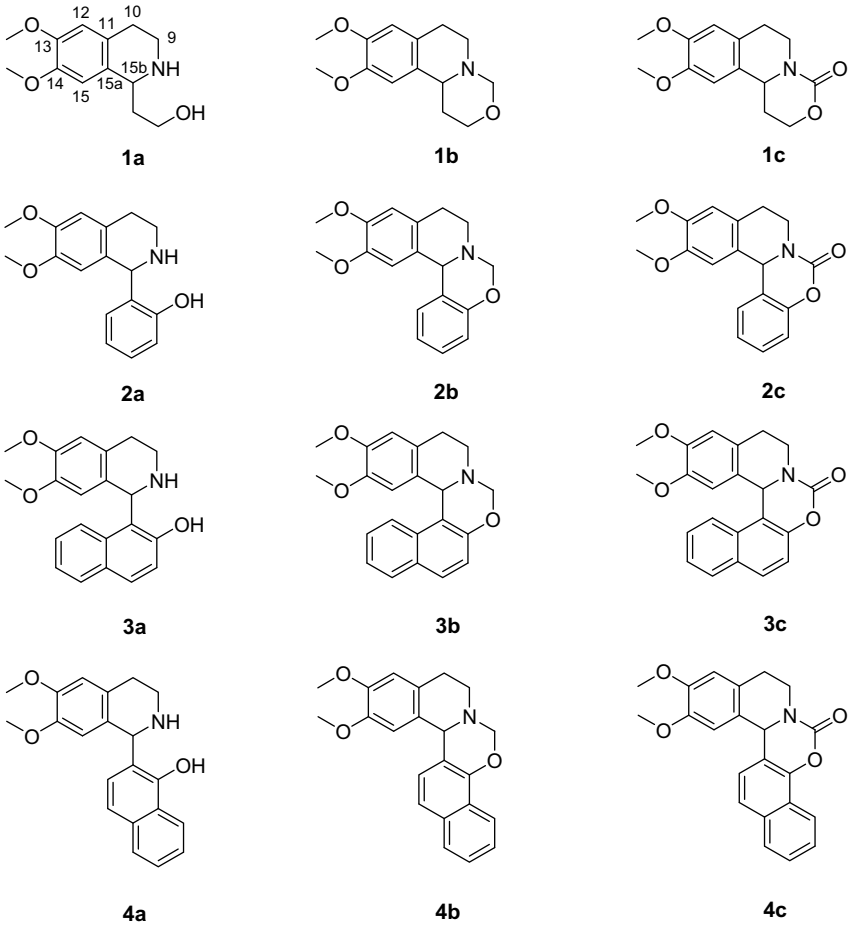

Scheme 1. Compounds studied. For a better comparison, the atoms in **1a**–**c**, **2a**–**c**, **3a**, and **4a** are denoted by using the numbering of the naphth[1,2-*e*]- and naphth[2,1-*e*]-[1,3]oxazino[4,3-*a*]isoquinoline ring systems (**3b**,**c** and **4b**,**c**).

2. Results and discussion

2.1. Synthesis and conformational analysis of the compounds studied

The synthesis and conformational analysis of naphth[1,2-*e*]-(**3b**,**c**) and naphth[2,1-*e*][1,3]oxazino[4,3-*a*]isoquinolines (**4b**,**c**), and the preparation of 1-(6,7-dimethoxy-1,2,3,4-tetrahydroisoquinolin-1-yl)-2-naphthol (**3a**) and 2-(6,7-dimethoxy-1,2,3,4-tetrahydroisoquinolin-1-yl)-1-naphthol (**4a**) were reported previously.[37] 2-(6,7-Dimethoxy-1,2,3,4-tetrahydroisoquinolin-1-yl)-ethanol (**1a**) and 2-(6,7-dimethoxy-1,2,3,4-tetrahydroisoquinolin-1-yl)phenol (**2a**) were synthesized according to literature procedures.[38,39] During the conformational analysis of **2b**,**c**, as expected, the same minimum-energy structures as obtained for **4b**,**c**[37] were computed: a twisted chair conformer for **2b** and a twisted-boat conformation for **2c** (cf. Fig. 1), in agreement with the experimental findings.[40]

Experimental and computational conformational analysis of **1a**–**4a**, starting materials for **2b**,**c**–**4b**,**c**, has not been carried out earlier. The results of the theoretical calculations were unequivocal: the same minimum energy structure was obtained for each derivative (given in Fig. 2): the 15b*S*,9*S* isomers involving the intramolecular hydrogen bond between the hydroxy group and the nitrogen lone pair (cf. Fig. 2). Experimental proof comes from the proton NMR spectra of **2a**–**4a**: the protons at C-9 and C-10 are positioned in *gauche* fragments [C(11)–C(10)–C(9)–N] and exhibit characteristic H,H coupling constants (J_{gem}=−11.7 and −15.8 Hz, respectively; $J_{ax,ax}$=8.6 Hz, $J_{ax,eq}$ and $J_{eq,eq}$=5.3 and 4.6 Hz, respectively) and only H-9(ax) reveals NOE to H-15b. Further NOEs of H-15b to H-9 and H-10 could not be detected, but the NOEs of H-15b to H-9(ax) and of H-12 to the two H-10 protons prove the unequivocal assignment of H-9(ax). Moreover, δ(OH) was found at 11–12 ppm (broadened at room temperature), which is characteristic for intramolecular hydrogen-bonding, as computed.

With respect to the conformations of the two methoxy groups in **1**–**4**, both in-plane (0°) and out-of plane conformations (90°) were obtained, which increased the number of conformers for the various diastereomers; in each case, however, the in-plane/in-plane conformers[41] were found to be the most stable and were used as basis structures for the forthcoming anisotropy study.

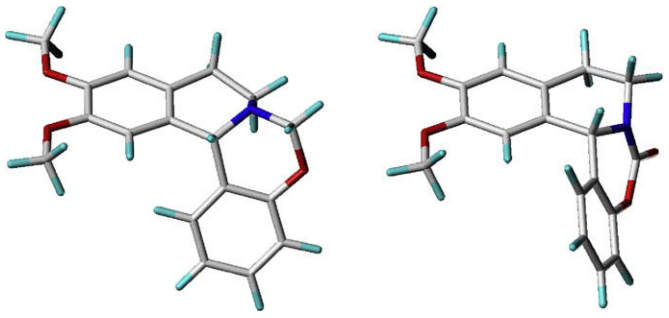

Figure 1. Minimum-energy structures of **2b** (left), a twisted chair conformer, and **2c** (right), a twisted-boat conformation, as obtained at the B3LYP/6-31G* level of theory.

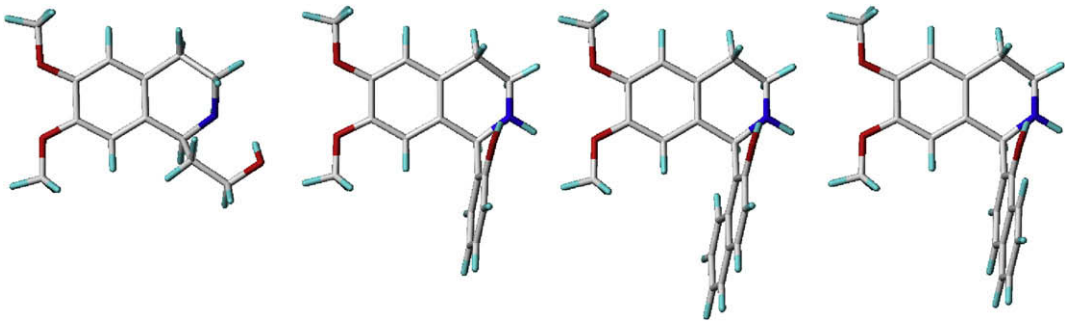

Figure 2. Minimum-energy structures of **1a**–**4a** (from left to right), as obtained at the B3LYP/6-31G* level of theory.

2.2. ^{1}H chemical shifts

The protons in **1**–**4** whose chemical shifts are compared in the following study are the isoquinoline protons H-15 and H-12 and the methoxy protons 13-OMe and 14-OMe. The chemical shifts of these ring and methyl protons are given in Table 1 together with the computed values and the data are correlated with each other (cf. Fig. 3). The agreement between the theoretically calculated and experimental values is excellent [$\delta_{exp.}$=1.1347δ_{calcd}−0.2394 (R^2=0.9974)], particularly with regard to the fact that the theoretical δ values were computed for molecules in the gas phase, but those measured experimentally[36,37,42] related to solution. Besides the additional fact that the ring interconversion of **1**–**4** at room temperature is fast on the NMR time-scale, the theoretically calculated geometries of these isoquinoline derivatives obviously dominate over the magnetic properties and the medium proves to be of only minor influence. Furthermore, this agreement between the computed and experimental ^{1}H chemical shifts strongly support the geometries calculated for the molecules.

The strongest variation of the proton resonances in the ^{1}H NMR spectra of **1**–**4** was observed for H-15b ($\Delta\delta$=1.00 ppm), followed by

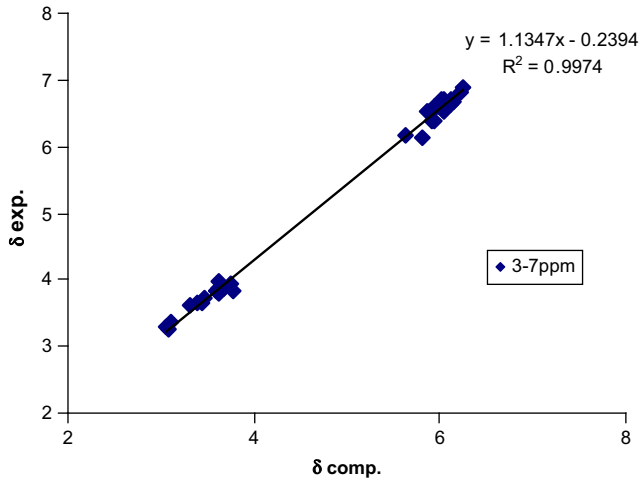

Figure 3. Correlation of the experimental chemical shifts of H-12, the 13-OMe, and 14-OMe protons and H-15 in **1a**–**c** to **4a**–**c** versus the computed δ values.

Table 1
Experimental chemical shifts (δ) of H-12, H-15, 12-OMe, and 14-OMe, chemical shift differences $\Delta\delta$ of these protons in **1a**–**c** with respect to **2a**–**c**, **3a**–**c**, and **4a**–**c**, respectively, and the corresponding anisotropic effects/ppm of the aromatic moieties in **2**–**4** on these protons

	1a δ/ppm	Δδ/ppm	Anisotropic effect/ppm	Steric compression	**1b** δ/ppm	Δδ/ppm	Anisotropic effect/ppm	Steric compression	**1c** δ/ppm	Δδ/ppm	Anisotropic effect/ppm	Steric compression
H-12	6.57	-	-		6.61	-	-		6.64	-	-	
13-OMe	3.85*	-	-		3.85*	-	-		3.87*	-	-	
14-OMe	3.83*	-	-		3.84*	-	-		3.86*	-	-	
H-15	6.53	-	-		6.52	-	-		6.60	-	-	
	2a				**2b**				**2c**			
H-12	6.61	+0.04	-0.03		6.65	+0.04	-0.02		6.70	+0.06	-0.04	
13-OMe	3.85	-	+0.01		3.86	+0.01	-0.02		3.87	-	+0.01	
14-OMe	3.66	-0.17	+0.33	+0.16	3.94	+0.10	-0.09		3.74	-0.12	+0.20	+0.08
H-15	6.37	-0.16	+0.76	+0.60	6.80	+0.28	-0.32		6.59	-0.01	+0.37	+0.36
	3a				**3b**				**3c**			
H-12	6.70	+0.13	-0.07		6.67	+0.06	-0.09		6.72	+0.08	-0.08	
13-OMe	3.80	-0.05	+0.01		3.86	+0.01	-0.01		3.85	+0.02	+0.01	
14-OMe	3.26	-0.57	+0.66	+0.09	3.35	-0.49	+0.59	+0.10	3.30	-0.56	+0.68	+0.12
H-15	6.14	-0.39	+0.95	+0.56	6.52	-	+0.71	+0.71	6.18	-0.41	+0.76	+0.35
	4a				**4b**				**4c**			
H-12	6.62	+0.05	-0.06		6.66	+0.05	-0.04		6.70	+0.04	-0.06	
13-OMe	3.84	+0.01	0.01		3.87	+0.02	-0.03		3.86	-0.01	+0.01	
14-OMe	3.61	-0.22	+0.39	+0.17	3.98	+0.14	-0.14		3.67	-0.19	+0.22	+0.03
H-15	6.40	-0.13	+0.71	+0.59	6.90	+0.38	-0.43		6.61	+0.01	+0.30	+0.31

*Or reversed.

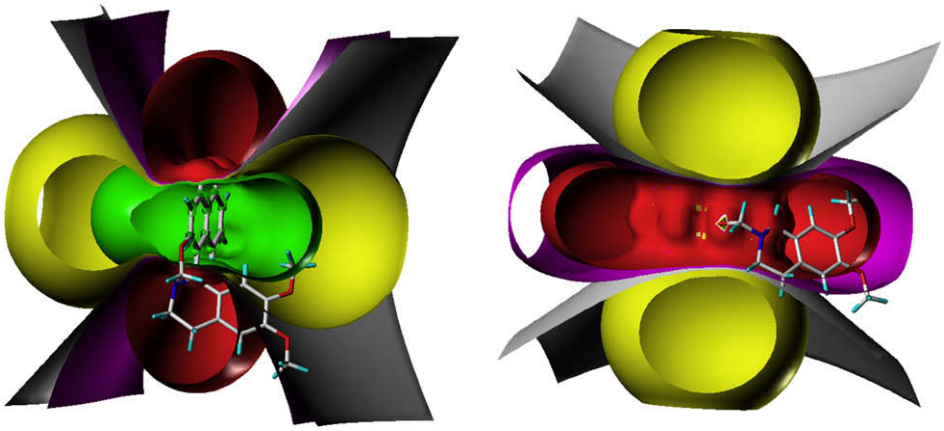

Figure 4. Visualization of the TSNMRSs (ICSSs: blue represents 5 ppm shielding, cyan 2 ppm shielding, green-blue 1 ppm shielding, green 0.5 ppm shielding, yellow 0.1 ppm shielding, red −0.1 ppm deshielding and magenta −0.01 ppm deshielding) of the minimum-energy structures of **3b** (left) and **4b** (right).

H-15 (0.58 ppm) and 14-OMe (0.72 ppm); smaller changes were observed for H-12 (0.15 ppm) and 13-OMe (0.07 ppm). Especially the broad range of chemical shifts of the 14-OMe protons in these isoquinoline derivatives encouraged us to study this phenomenon in more detail. While H-15b is too proximal[3] to the aromatic moieties in **2**–**4** to be included on the anisotropy study (vide infra), the other four should be suitable; further, H-15b and 14-OMe should be proximal enough to be additionally influenced by steric compression and a competition can be expected. A detailed study of this is another topic of this paper.

2.3. Anisotropic effects of aromatic moieties in 2–4 on the ^{1}H chemical shifts of the isoquinoline protons

TSNMRs for **2**–**4** were calculated as described above, and can be easily visualized by different ICSSs.[3] Figure 4 depicts the corresponding illustrations for **3b** and **4b**; similar representations for the other compounds studied (**2**–**4**) can readily be drawn. These two compounds were selected for presentation because of the different signs of the anisotropic effects of the α-naphthyl moieties in the two compounds on the chemical shifts of 14-OMe and H-15. In **3b**, both the 14-OMe protons and H-15 are positioned in the shielding ICSS=+0.5 ppm (green) [cf. Table 1: anisotropic effect Δδ (14-OMe)=0.59 ppm; Δδ (H-15)=0.71 ppm], while in **4b** the corresponding protons are no longer shielded by the anisotropic effect of α-naphthyl, but are deshielded [cf. Table 1: anisotropic effect Δδ (14-OMe)=−0.14 ppm; Δδ (H-15)=−0.43 ppm], due to the position in the deshielding belt (red) of this aromatic moiety. In this way, all anisotropic effects on the certain protons were taken from the corresponding TSNMRS grids and are given in Table 1 together with the experimental δ values and the differences in the δ values (Δδ) of the isoquinoline protons H-12, 13-OMe, 14-OMe and H-15 in **1a**–**c** and **2a**–**c**, **3a**–**c** and **4a**–**c**, respectively.

A critical comparison of the experimental chemical shift differences Δδ with the anisotropic effect thus obtained appears equivocal. If only this anisotropic effect is responsible for the experimental Δδ values a complete (within the margin of error of the DFT study) agreement between the pairs of values can be expected. However, this is not generally the case: it depends on the proton inspected.

H-12: The anisotropic effect on H-12 was found to be minor and generally in the low field direction (Δδ=−0.02 to −0.09 ppm), in total agreement with the sign of the experimental Δδ (=0.04–0.13 ppm). Additionally, the relative size of Δδ and the anisotropic effect proved consistent: the strongest effects were observed in **3** [Δδ=0.06–0.13 ppm; anisotropic effect=−0.07 to −0.09 ppm] and the smallest ones in **2** [Δδ=0.04–0.06 ppm; anisotropic effect=−0.02 to −0.04 ppm]. *Obviously, H-12 is excellently suited to reveal quantitatively the anisotropic effect of the aromatic moiety in **2**–**4** on the isoquinoline moieties.*

13-OMe: These methoxy groups in **2**–**4** are turned away from the aromatic moieties, which cause the anisotropic substituent effects; therefore, the effect is almost negligible. However, even though small, both the experimental Δδ values and the anisotropic effects are generally parallel in sign and size [Δδ=−0.05 to 0.02 ppm; anisotropic effect=0.01 to −0.03 ppm].

14-OMe: In contrast, 14-OMe in **2**–**4** are turned toward the aromatic moieties and show the strongest effects of all [$\Delta\delta_{exp.}$=−0.57 to 0.14 ppm; anisotropic effect=0.68 to −0.14 ppm]. These chemical shift ranges are comparable and generally point in the same direction, but the anisotropic effects are up to 0.17 ppm smaller than the experimental Δδ values (cf. Table 1). There must be an additional influence on the proton chemical shifts of 14-OMe, which was identified to be the steric compression[43] of these protons subject to the proximal aromatic moieties in **2**–**4** (vide infra). However, in spite of this peculiarity, the anisotropic effects of the aromatic moieties in **2**–**4** on δ(14-OMe) are correctly (in direction to high or low field, but reduced in size) indicated by the experimental Δδ values and prove that not only H-12 and 13-OMe, but also 14-OMe is a useful indication of the anisotropic substituent influences in **2**–**4**.

H-15: For H-15, which are positioned nearest to the aromatic moieties in **2**–**4**, (as expected and inherent) the largest anisotropic effects were computed (−0.32 to 0.95 ppm). The experimental Δδ values, however, follow the sequences even less than the Δδ values of the 14-OMe protons, for the same reason as discussed previously (vide supra).

When the experimental Δδ values are compared with the corresponding anisotropic effects in **2**–**4**, an agreement in signs (to high/low field) of the two parameters is found, but the extents of the experimental deshielding (up to 0.38 ppm) and shielding Δδ values (−0.01 to −0.41 ppm) are smaller than the corresponding deshielding (−0.32 to −0.43 ppm) and shielding anisotropic effects (0.30–0.95 ppm) (cf. Table 1). This is in agreement with the effects observed for the chemical shift of the 14-OMe protons (vide supra) and points to the competing activity of steric compression on the chemical shifts of H-15. In the latter case, the competition will be studied in some detail.

(i) First, the experimental Δδ values were subtracted from the anisotropic effect computed (cf. Table 1; values in magenta). These differences, which should arise mainly from steric compression, are distinct for the various types of compounds studied. In **2c**, **3c**, and **4c**, they are 0.31–0.36 ppm, in **2a**, **3a**, and **4a** they are 0.56–0.60 ppm and in **2b**, **3b**, and **4b** they are even equivocal:

there are no such effects in **2b** and **4c**, but the strongest effect is observed in **3b**.

(ii) In search for the origin of these results, the geometries of **2**–**4** were carefully studied. Robust references to differences in steric compression could readily be found, e.g., the bond lengths $r_{C(15)-H}$ should parallel the steric hindrance, the shorter $r_{C(15)-H}$:

Compound	**2c**, **3c**, **4c**	**2a**, **3a**, **4a**	**2b**, **4b**	**3b**
$r_{C(15)-H}$	−0.001 to −0.002 Å	−0.002 Å	±0	−0.004 Å
Steric compression	0.31 to 0.36 ppm	0.56 to 0.60 ppm	0.04 ppm	0.71 ppm

The sequence of bond length shortening is in line with the increasing steric compression in these structural fragments: **3b**≫**2a**,**3a**,**4a**>**2c**,**3c**,**4c**>**2b**,**4b**. The strongest shortening of $r_{C(15)-H}$ is observed for **3b**, with almost no effect in the analogs **2b** and **4b**. If the bond angles $\angle_{C(15a)-C(15)-H(15)}$ and $\angle_{H(15)-C(15)-C(14)}$ are compared, which are similarly influenced by steric compression, the same activity is considered: $\angle_{C(15a)-C(15)-H(15)}$ is widened and $\angle_{H(15)-C(15)-C(14)}$ is diminished.

Compound	**2b**,**4b**	**3b**
$\angle_{C(15a)-C(15)-H(15)}$	118.82–118.83°	118.93°
$\angle_{H(15)-C(15)-C14)}$	119.60–119.62°	118.93°

To illustrate the difference in steric compression, the energy-minimum structures of **3b** and **4b** are compared in Figure 5; the hard steric compression in **3b**, but the strainless position of H-15 (in magenta) in **4b** is immediately visible, leading to the conclusions drawn from the geometry of the compounds studied.

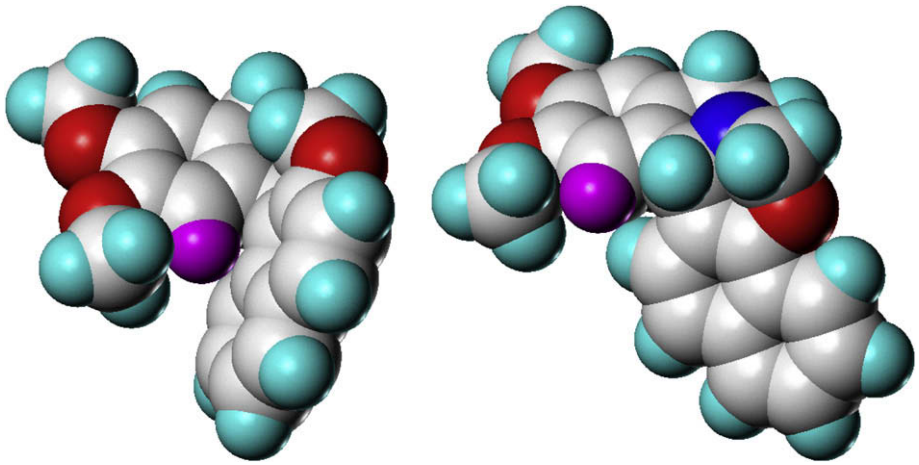

Figure 5. Minimum-energy structures of **3b** (left) and **4b** (right) as obtained at the B3LYP/6-31G* level of theory.

The same conclusion can be drawn for the other compounds from the changes in geometry (cf. Supplementary data).

3. Conclusions

For the series of 1,3-oxazino[4,3-*a*]isoquinolines **1**–**4**, the minimum-energy isomers/conformers were determined by NMR spectroscopy and theoretical calculations at the DFT level of theory. On the basis of these structures, the anisotropic effects of the aromatic moieties (phenyl in **2**, α-naphthyl in **3** and β-naphthyl in **4**) on the isoquinoline protons H-12 and H-15 and the methoxy protons 13-OMe and 14-OMe were computed via TSNMRS grids around the aromatic substituents. While H-12 and 13-OMe proved to be excellent indicators of the anisotropic effects in **2**–**4**, the values for H-15 and 14-OMe in these compounds were found to be smaller than the experimental $\Delta\delta$ values. As the reason for the differences between $\Delta\delta$ and the anisotropic effects of the aromatic moieties, steric compression[43] was identified, in agreement with the parallel structural changes of the geometries.

This approach for the quantitative separation of the anisotropic effects and the steric compression of the functional groups on the ^{1}H chemical shifts allowed a re-appraisal of some assertions in NMR textbooks (e.g., deshielding by 1.57 ppm of H-4 in 11-ethynylphenanthrene relative to its counterpart in phenanthrene was not found to be due to the anisotropy of the C≡C triple bond)[10] and the identification of a steric strain in a highly congested hydrocarbons,[19] and can be recommended as a generally applicable method.

4. Experimental

4.1. General

Melting points were determined on a Kofler micro melting apparatus and are uncorrected. Merck Kieselgel 60F_{254} plates were used for TLC.

^{1}H and ^{13}C NMR spectra were recorded in $CDCl_3$ (unless specified as CD_2Cl_2 or DMSO-d_6) solution in 5 mm tubes, at room temperature, on a 500 MHz NMR spectrometer at 500.17 (^{1}H) and 125.78 (^{13}C) MHz, with the deuterium signal of the solvent as the lock and TMS as the internal standard for ^{1}H, or the solvent as the internal standard for ^{13}C. All spectra (^{1}H, ^{13}C, gs-H,H-COSY, gs-HMQC, gs-1D-HMQC, gs-HMBC and NOESY) were acquired and processed with the standard software.

The quantum-chemical calculations were carried out with the Gaussian 03 program package.[44] Geometry optimizations were performed at the B3LYP/6-31G* level of theory[45] without restrictions. For **1**–**4**, the four 9,15b diastereomers were energy-optimized with respect to the preferred conformers and their relative energies were calculated; the predominant conformer of the most stable diastereomer was considered further.

The spatial magnetic properties (TSNMRS) were constructed,[3] using the NICS concept; the NICS values[2] were computed on the basis of the B3LYP/6-31G* geometries of **1**–**4** via the GIAO method[46,47] at the HF/6-31G* level of theory.[48] To calculate spatial NICS, ghost atoms were placed on a lattice of −10 Å to +10 Å with a step size of 0.5 Å in the three directions of the Cartesian coordinate system. The resulting 68,921 NICS values thus obtained were analyzed and visualized by means of the SYBYL 7.3 molecular modeling software;[49] different ICSSs of −0.01 ppm (magenta) and −0.1 ppm (red) deshielding, and 5 ppm (blue), 2 ppm (cyan), 1 ppm (green-blue), 0.5 ppm (green), and 0.1 ppm (yellow)

shielding are used to visualize the TSNMRS of **3b** and **4b** in Figure 4.

NMR chemical shifts were calculated by the GIAO method[46,47] at the B3LYP/6-31G* level of theory (the reference compound TMS was calculated at the same level). All calculations were carried out on SGI workstations and LINUX clusters.

The synthesis of naphth[1,2-*e*]- (**3b**,**c**) and naphth[2,1-*e*]-[1,3]oxazino[4,3-*a*]isoquinolines (**4b**,**c**), and the preparation of 1-(6,7-dimethoxy-1,2,3,4-tetrahydroisoquinolin-1-yl)-2-naphthol (**3a**) and 2-(6,7-dimethoxy-1,2,3,4-tetrahydroisoquinolin-1-yl)-1-naphthol (**4a**) were reported previously.[37] 2-(6,7-Dimethoxy-1,2,3,4-tetrahydroisoquinolin-1-yl)ethanol (**1a**) and 2-(6,7-dimethoxy-1,2,3,4-tetrahydroisoquinolin-1-yl)phenol (**2a**) were synthesized according to literature procedures.[38,39]

4.2. 9,10-Dimethoxy-1,6,7,11b-tetrahydro-2*H*,4*H*-1,3-oxazino[4,3-*a*]isoquinoline (1b)

To a solution of amino alcohol **1a** (0.71 g, 3 mmol) in MeOH (10 mL), 36% formaldehyde solution (0.5 mL) was added. The mixture was allowed to stand at room temperature for 1 h, then poured into H_2O (50 mL) and extracted with CH_2Cl_2 (3×25 mL). The combined organic extracts were dried (Na_2SO_4) and evaporated. The oily product crystallized on treatment with Et_2O. The crystals were filtered off and recrystallized from *i*-Pr_2O. Yield: 0.61 g (82%), mp 102–103 °C.

4.3. 9,10-Dimethoxy-1,6,7,11b-tetrahydro-2*H*,4*H*-1,3-oxazino[4,3-*a*]isoquinolin-4-one (1c)

To a stirred mixture of amino alcohol **1a** (1.19 g, 5 mmol), toluene (30 mL), $NaHCO_3$ (0.63 g, 7.5 mmol), and H_2O (30 mL), ethyl chloroformate (0.60 g, 5.5 mmol) was added and the mixture was stirred at room temperature for 1 h. The organic layer was separated and the aqueous layer was extracted with EtOAc (3×30 mL). The combined extracts were dried (Na_2SO_4) and evaporated to yield 1.50 g (97%) of ethyl 1-(2′-hydroxyethyl)-6,7-dimethoxy-1,2,3,4-tetrahydroisoquinoline-2-carboxylate as an oily product, which was used in the next step without further purification.

The previous urethane derivative (1.00 g, 3.2 mmol) was thoroughly mixed with NaOMe (0.18 g, 3.3 mmol) and the mixture was kept under N_2 at 130 °C for 45 min. The melt was extracted with hot EtOAc (5×30 mL), and the combined organic phases were washed with 5% HCl (2×30 mL) and H_2O (2×30 mL), dried (Na_2SO_4), and evaporated. The oily residue crystallized on treatment with Et_2O. The crystals were filtered off and recrystallized from *i*-Pr_2O. Yield: 0.44 g (52%), mp 119–121 °C.

4.4. 11,12-Dimethoxy-8,9-dihydro-6*H*,13b*H*-isoquino[2,1-*c*]-[1,3]benzoxazine (2b)

To a stirred suspension of amino phenol **2a** (1.14 g, 4 mmol) in EtOH (10 mL) 36% formaldehyde solution (10 mL) was added and the mixture was stirred at room temperature for 30 min. The crystalline product was filtered off, washed with H_2O and recrystallized from EtOAc. Yield: 0.79 g (66%), mp: 213–216 °C.

4.5. 11,12-Dimethoxy-8,9-dihydro-6*H*,13b*H*-isoquino[2,1-*c*]-[1,3]benzoxazin-6-one (2c)

To a mixture of amino phenol **2a** (1.14 g, 4 mmol), Et_3N (0.81 g, 8 mmol), and dry toluene (20 mL), a 20% solution of phosgene in toluene (2.0 mL, 4 mmol) was added and the suspension was stirred at room temperature for 2 h. EtOAc (100 mL) was added and the organic phase was washed with 5% HCl (2×30 mL) and then with H_2O (2×30 mL). The organic phase was dried (Na_2SO_4) and evaporated, resulting in an oil, which became crystalline on treatment with Et_2O. The crystals were filtered off and recrystallized from EtOH. Yield: 0.67 g (54%), mp: 189–190 °C.

Supplementary data

Absolute energies, bond angles and bond distances, and *x*,*y*,*z*-coordinates at the B3LYP/6-31G* level of theory for **1**–**4**. Supplementary data associated with this article can be found in the online version, at doi:10.1016/j.tet.2009.07.038.

References and notes

1. Chen, Z.; Wannere, C. S.; Corminboeuf, C.; Puchta, R.; von Ragué Schleyer, P. *Chem. Rev.* **2005**, *105*, 3842.
2. von Ragué Schleyer, P.; Manoharan, M.; Wang, Z. X.; Kiran, B.; Jiao, Y.; Puchta, R.; van E. Hommes, N. J. R. *Org. Lett.* **2001**, *3*, 2465.
3. Klod, S.; Kleinpeter, E. *J. Chem. Soc., Perkin Trans. 2* **2001**, 1893.
4. Tóth, G.; Kovács, J.; Lévai, A.; Koch, A.; Kleinpeter, E. *Magn. Reson. Chem.* **2001**, *39*, 251.
5. Kleinpeter, E.; Holzberger, A. *Tetrahedron* **2001**, *57*, 6941.
6. Germer, A.; Klod, S.; Peter, M. G.; Kleinpeter, E. *J. Mol. Model.* **2002**, *8*, 231.
7. Klod, S.; Koch, A.; Kleinpeter, E. *J. Chem. Soc., Perkin Trans. 2* **2002**, 1506.
8. Kovács, J.; Tóth, G.; Simon, A.; Lévai, A.; Koch, A.; Kleinpeter, E. *Magn. Reson. Chem.* **2003**, *41*, 193.
9. Kleinpeter, E.; Klod, S.; Rudorf, W.-D. *J. Org. Chem.* **2004**, *69*, 4317.
10. Kleinpeter, E.; Klod, S. *J. Am. Chem. Soc.* **2004**, *126*, 2231.
11. Szatmári, I.; Martinek, T. A.; Lázár, L.; Koch, A.; Kleinpeter, E.; Neuvonen, K.; Fülöp, F. *J. Org. Chem.* **2004**, *69*, 3645.
12. Kleinpeter, E.; Klod, S. *J. Mol. Struct.* **2004**, *704*, 79.
13. Ryppa, C.; Senge, M. O.; Hatscher, S. S.; Kleinpeter, E.; Wacker, Ph.; Schilde, U.; Wiehe, A. *Chem.—Eur. J.* **2005**, *11*, 3427.
14. Kleinpeter, E.; Schulenburg, A.; Zug, I.; Hartmann, H. *J. Org. Chem.* **2005**, *70*, 6592.
15. Kleinpeter, E.; Schulenburg, A. *J. Org. Chem.* **2006**, *71*, 3869.
16. Heydenreich, M.; Koch, A.; Klod, S.; Szatmári, I.; Fülöp, F.; Kleinpeter, E. *Tetrahedron* **2006**, *62*, 11081.
17. Rašović, A.; Steel, P. J.; Kleinpeter, E.; Marković, R. *Tetrahedron* **2007**, *63*, 1937.
18. Kleinpeter, E.; Koch, A.; Sahoo, H. S.; Chand, D. K. *Tetrahedron* **2008**, *64*, 5044.
19. Kleinpeter, E.; Koch, A.; Seidl, P. R. *J. Phys. Chem. A* **2008**, *112*, 4989.
20. Kleinpeter, E.; Klod, S.; Koch, A. *J. Mol. Struct. (THEOCHEM)* **2007**, *811*, 45 and references therein.
21. Kleinpeter, E.; Klod, S.; Koch, A. *J. Mol. Struct. (THEOCHEM)* **2008**, *857*, 89.
22. Kleinpeter, E.; Koch, A.; Shainyan, B. A. *J. Mol. Struct. (THEOCHEM)* **2008**, *863*, 127.
23. Kleinpeter, E.; Koch, A. *J. Mol. Struct. (THEOCHEM)* **2008**, *851*, 313.
24. Kleinpeter, E.; Klod, S.; Koch, A. *J. Org. Chem.* **2008**, *73*, 1498.
25. Alkorta, I.; Elguero, J. *New J. Chem.* **1998**, 381.
26. (a) Martin, N. H.; Allen, N. W., III; Moore, K. D.; Vo, L. *J. Mol. Struct. (THEOCHEM)* **1998**, *454*, 161; (b) Martin, N. H.; Allen, N. W., III; Minga, E. K.; Ingrassia, S. T.; Brown, J. D. *Proceedings of ACS Symposium, Modeling NMR Chemical Shifts: Gaining Insight into Structure and Environment*; ACS: Washington, 1999.
27. (a) Waugh, J. S.; Fessenden, R. W. *J. Am. Chem. Soc.* **1957**, *79*, 846; (b) Johnson, C. E.; Bovey, F. A. *J. Chem. Phys.* **1958**, *29*, 1012; (c) Jonathan, N.; Gordon, S.; Dailey, B. P. *J. Chem. Phys.* **1962**, *36*, 2443; (d) Barfield, M.; Grant, D. M.; Ikenberry, D. *J. Am. Chem. Soc.* **1975**, *97*, 6956; (e) Agarwal, A.; Barnes, J. A.; Fletcher, J. L.; McGlinchey, M. J.; Saver, B. G. *Can. J. Chem.* **1977**, *55*, 2575; (f) Haigh, C. W.; Mallion, R. B. *Progress in NMR Spectroscopy*; Pergamon: New York, NY, 1980; Vol. 13, p 303.
28. Haigh, C. W.; Mallion, R. B. *Mol. Phys.* **1971**, *22*, 955.
29. (a) Haigh, C. W.; Mallion, R. B. *Org. Magn. Reson.* **1972**, *4*, 203; (b) Dailey, B. P. *J. Chem. Phys.* **1964**, *41*, 2304.
30. (a) Fallah-Bagher-Shaidaei, H.; Wannere, C. S.; Corminboeuf, C.; Puchta, R.; von Ragué Schleyer, P. *Org. Lett.* **2006**, *8*, 863; (b) Corminboeuf, C.; Heine, T.; Seifert, G.; von Ragué Schleyer, P.; Weber, J. *PhysChemChemPhys* **2004**, *6*, 273.
31. Stanger, A. *Chem.—Eur. J.* **2006**, *12*, 2745.
32. (a) Lazzeretti, P. *PhysChemChemPhys* **2004**, *6*, 217; (b) Stanger, A. *Chem. Commun.* **2009**, 1939.
33. Martzin, N. H.; Brown, J. D.; Nance, K. H.; Schaefer, H. F., III; von Ragué Schleyer, P.; Wang, Z.-X.; Woodcock, H. L. *Org. Lett.* **2001**, *3*, 3823.
34. Pelloni, St.; Lazzeretti, P.; Zanasi, R. *J. Phys. Chem. A* **2007**, *111*, 8163.
35. Martin, N. H.; Loveless, M. M.; Main, K. L.; Wade, D. C. *J. Mol. Graph. Model.* **2006**, *25*, 389.
36. Heydenreich, M.; Koch, A.; Lázár, L.; Szatmári, I.; Sillanpää, R.; Kleinpeter, E.; Fülöp, F. *Tetrahedron* **2003**, *59*, 1951.
37. Heydenreich, M.; Koch, A.; Szatmári, I.; Fülöp, F.; Kleinpeter, E. *Tetrahedron* **2008**, *64*, 7378.
38. Tietze, L. F.; Rackelmann, N.; Müller, I. *Chem.—Eur. J.* **2004**, *10*, 2722.
39. Weinbach, E. C.; Hartung, W. H. *J. Org. Chem.* **1950**, *15*, 676.
40. As observed for **4b**,[37] no NOEs were found between H-15b and H-10 or H-11 in **2b**; the corresponding distances are too long to generate NOE enhancements in the NMR spectra. NOE between H-15b and the *syn*-positioned H-8 could not be observed in the NOESY spectrum because of identical proton chemical shifts. In

2c, as in **4c**, a short distance between H-15b and H-9(*syn*) corroborates the experimentally found NOE enhancement.
41. The preferred conformation of **1**–**4** with respect to the methoxy groups is in-plane/in-plane as concerns 13-OMe directed to H-12 and 14-OMe directed to H-15.
42. This study.
43. Pihlaja, K.; Kleinpeter, E. *Carbon-13 NMR Chemical Shifts in Structural and Stereochemical Analysis, Methods in Stereochemical Analysis*; VCH: New York, NY, 1994.
44. Frisch, M. J.; Trucks, G. W.; Schlegel, H. B.; Scuseria, G. E.; Robb, M. A.; Cheeseman, J. R.; Montgomery, J. A., Jr.; Vreven, T.; Kudin, K. N.; Burant, J. C.; Millam, J. M.; Iyengar, S. S.; Tomasi, J.; Barone, V.; Mennucci, B.; Cossi, M.; Scalmani, G.; Rega, N.; Petersson, G. A.; Nakatsuji, H.; Hada, M.; Ehara, M.; Toyota, K.; Fukuda, R.; Hasegawa, J.; Ishida, M.; Nakajima, T.; Honda, Y.; Kitao, O.; Nakai, H.; Klene, M.; Li, X.; Knox, J. E.; Hratchian, H. P.; Cross, J. B.; Adamo, C.; Jaramillo, J.; Gomperts, R.; Stratmann, R. E.; Yazyev, O.; Austin, A. J.; Cammi, R.; Pomelli, C.; Ochterski, J. W.; Ayala, P. Y.; Morokuma, K.; Voth, G. A.; Salvador, P.; Dannenberg, J. J.; Zakrzewski, V. G.; Dapprich, S.; Daniels, A. D.; Strain, M. C.; Farkas, O.; Malick, D. K.; Rabuck, A. D.; Raghavachari, K.; Foresman, J. B.; Ortiz, J. V.; Cui, Q.; Baboul, A. G.; Clifford, S.; Cioslowski, J.; Stefanov, B. B.; Liu, G.; Liashenko, A.; Piskorz, P.; Komaromi, I.; Martin, R. L.; Fox, D. J.; Keith, T.; Al-Laham, M. A.; Peng, C. Y.; Nanayakkara, A.; Challacombe, M.; Gill, P. M. W.; Johnson, B.; Chen, W.; Wong, M. W.; Gonzalez, C.; Pople, J. A. *Gaussian 03, Revision B.03*; Gaussian: Pittsburgh, PA, 2003.
45. Hehre, J. W.; Radom, L.; von Ragué Schleyer, P.; Pople, J. A. *Ab Initio Molecular Orbital Theory*; Wiley & Sons: New York, NY, 1986.
46. Møller, C.; Plesset, M. S. *Phys. Rev.* **1934**, *46*, 618.
47. Ditchfield, J. R. *Mol. Phys.* **1974**, *27*, 789.
48. The lattice points (ghost atoms) should be sensor points only without energy contribution in the present calculations. Only if HF calculations are applied this is true; in the case of electron correlation calculations, the ghost atoms acquire their own electron density and display some influence on the energy of the studied molecule. In these cases, the TSNMRS surfaces are heavily distorted.
49. SYBYL 7.3 Tripos, 1699 South Hanley Road, St. Louis, MO 63144, USA, 2007.